



**HAL**  
open science

## Modelling of the ultrasonic response of inclusions in steels

Michel Darmon, Pierre Calmon, Bertrand Bèle

► **To cite this version:**

Michel Darmon, Pierre Calmon, Bertrand Bèle. Modelling of the ultrasonic response of inclusions in steels. AIP Conference Proceedings, 2003, 657, pp.101-108. hal-00431707

**HAL Id: hal-00431707**

**<https://hal.science/hal-00431707>**

Submitted on 22 Jan 2024

**HAL** is a multi-disciplinary open access archive for the deposit and dissemination of scientific research documents, whether they are published or not. The documents may come from teaching and research institutions in France or abroad, or from public or private research centers.

L'archive ouverte pluridisciplinaire **HAL**, est destinée au dépôt et à la diffusion de documents scientifiques de niveau recherche, publiés ou non, émanant des établissements d'enseignement et de recherche français ou étrangers, des laboratoires publics ou privés.

# MODELLING OF THE ULTRASONIC RESPONSE OF INCLUSIONS IN STEELS.

Michel Darmon<sup>1</sup>, Pierre Calmon<sup>1</sup> and Bertrand Bèle<sup>2</sup>

<sup>1</sup>French Atomic Energy Commission, CEA/LIST, CEA Saclay Bât. 611, 91191 Gif-sur-Yvette Cedex – France.

<sup>2</sup>IRSID, Arcelor Group, Voie Romaine BP 30320 57283 Maizières-les-Metz Cedex–France.

**ABSTRACT.** We present a study performed to model and predict the ultrasonic response of alumina inclusions in steels. The Born and the extended quasistatic approximations have been applied and modified to improve their accuracy in the framework of this application. The modified Born approximation, allowing to deal with various inclusion shapes, have been selected to be implemented in the CIVAS software. The model reliability have been evaluated by comparison with Ying and Truell's exact analytical solution. In parallel, measurements have been carried out upon both natural and artificial alumina inclusions.

## INTRODUCTION

Ultrasonic techniques are applied in the steel industry in the aim of controlling the quality of the produced steel. The inclusions are the defects which are searched for. The harmfulness of these flaws depends on several factors such as its composition, shape, size, position in the product. Therefore it is of great interest to ensure the ability of the methods to detect and characterize these flaws. That means firstly to distinguish inclusions responses from other ultrasonic diffraction sources such as porosity echoes or microstructural noise. In this context, modelling appears to be an efficient technique to reach this goal and to improve methods of inspection and data analysis.

This paper describes a modelling study performed in the framework of a collaboration between CEA (French Atomic Energy Commission) and IRSID (Research Center of ARCELOR company). The flaws under study here are alumina inclusions from 20  $\mu\text{m}$  to 1mm. The inspections are performed with ultrasonic focused probes functioning in pulse echo mode, the frequency being either 10 or 50 MHz depending on the size range of the defects which are searched for. From a review of the existing approaches, the two low-frequency approximations have been selected : the Born approximation and the extended quasistatic approximation 1. These approaches have been modified in order to improve their accuracy in the domain of application under consideration. The modification led to describe the wave propagation in the flaw by taking into account both density and wave velocity differences between the host medium and the inclusion. The accuracy of

these approximated models, has been evaluated in the case of a spherical scatterer by comparison with the exact analytical solution developed by Ying and Truell [2].

The modified Born approximation and the Ying and Truell model have been both implemented in the CIVA software platform[3]. This integration allows the connection of the inclusion-wave interaction model to the transducer field computation available in CIVA, and therefore enables the simulation of a real inspection by taking into account the probe characteristics.

In order to experimentally validate the models, artificial alumina inclusions have been manufactured by diffusion welding. We also compared simulated and experimental results obtained on real flaws detected by ultrasound and characterized by X-rays. In both cases, measurements are presented and compared with the simulation.

## CIVA SIMULATION APPROACH

To model the whole configuration requires to take into account the interaction between the beam and the flaw, the radiation by the probe, the propagation and the reception of the ultrasonic wave. The CIVA software platform developed at the French Atomic Energy Commission enables to model all these effects : it includes two tools of ultrasonic modelling “*Champ-Sons*” and “*Mephisto*”[4,5].

First, *Champ-Sons* computes the transmitted field in the specimen after propagating in the coupling medium (here water as shown in Figure 1). In this study, we are only interested in plane specimen but henceforth complex blocks defined by CAD [6] or heterogeneous and anisotropic media [7] are able to be treated. The *Champ-Sons* model is based on an integral formulation of the field transmitted by the component which can be seen as an extension of the Rayleigh-Sommerfield expression established in the acoustic case. The field is obtained by summing all the contributions arising from infinitesimal surface elements distributed on the emitting surface. In this aim is applied a so-called pencil method and the acoustical version of the geometrical optics approximation. We can therefore express the velocity potential  $\Phi$  radiated by the probe here in normal incidence :

$$\Phi(M,t) = \int_{\text{transmitter}} C_{iL}^{\phi,\psi}(\theta_i,t) * \frac{v_0(t-T)}{2\pi R_e} ds \quad (1)$$

where  $v_0(t)$  is the normal component of the velocity on the surface of the probe, T is the time of flight between the source and M;  $C_{iL}^{\phi,\psi}(\theta_i,t)$  is the transmission coefficient at the liquid-solid interface and  $R_e$  is the divergence factor.

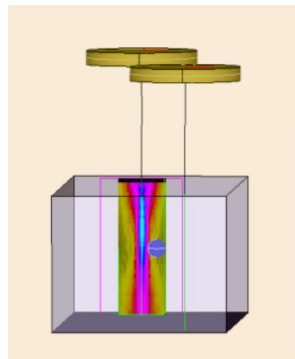


FIGURE 1. Ultrasonic testing inspection.

Then the Mephisto code is used to calculate the echoes backscattered by a flaw. We report here the main general assumptions applied to deal with the application under consideration: First the ultrasonic field radiated by the transducer and computed by *Champ-Sons* is approached by the product of a spatial function  $q(\rho, \alpha, z)$  describing the amplitude distribution in the beam and a time-dependent function describing the wave propagation. The transducer being a focused one, we assume that the wave fronts in the beam are plane. The incident field on the flaw can therefore be approximated as:

$$\Phi(M, t) = q(\rho, \alpha, z)\Phi_0(t - \Delta t) \quad (2)$$

in which  $(\rho, \alpha, z)$  are the cylindrical co-ordinates of the point  $M$  in a beam-referenced system. That is,  $\rho$  measures the distance to the focal axis,  $\alpha$  is the angle between the plane of incidence and the vector joining the point  $M$  and the focal axis,  $z$  is the distance along the focal axis and  $\Delta t = \frac{H}{c} + \frac{z}{c_{1L}}$ ,  $H$  being the coupling medium height (here water). The functions  $q(\rho, \alpha, z)$  and  $\Phi_0(t)$  are model inputs extracted from the *Champ-Sons* calculation.

In the next section, we will point out in details the beam-inclusion models we applied. Let just say here that the flaw is assumed to scatter, at a point  $M'$  in steel, a spherical wave which is characterized by a certain directivity  $\tilde{A}(M, \theta, \varphi, t)$  :

$$\Phi^{diffr}(M', t) = A(M, \theta, \varphi, t) * \frac{\Phi(M, t - \frac{r}{c_{1L}})}{r} \quad (3)$$

$A(M, \theta, \varphi, t) = \left\{ TF^{-1}[A(M, \theta, \varphi, \nu)] \right\}$  is the inverse Fourier transform of the spectral scattering coefficient  $A(M, \theta, \varphi, \nu)$  and  $*$  represents the convolution in the time domain.

Lastly, by assuming the transmission-reception reciprocity of the probe and in addition, by neglecting the variations of the directivity function  $A(M, \theta, \varphi, t)$  on the surface of the receiver which is quite justified in a far field configuration, we can express the echo backscattered by the flaw by :

$$S(t) \propto \frac{\partial}{\partial t} A(M, t) * \left( \Phi_0(t - 2\Delta t) \tilde{q}^2(\rho, \alpha, z) \right) \quad (4)$$

## MODELLING OF THE BEAM-INCLUSION INTERACTION

The aim of the modelling study is to obtain the backscattering coefficient  $A(M, \nu)$  for longitudinal wave of an alumina inclusion in steel which could be connected to the general approach described above. The requirement of intensive parametrical computations has led us to select analytical or approximated semi-analytical theories.

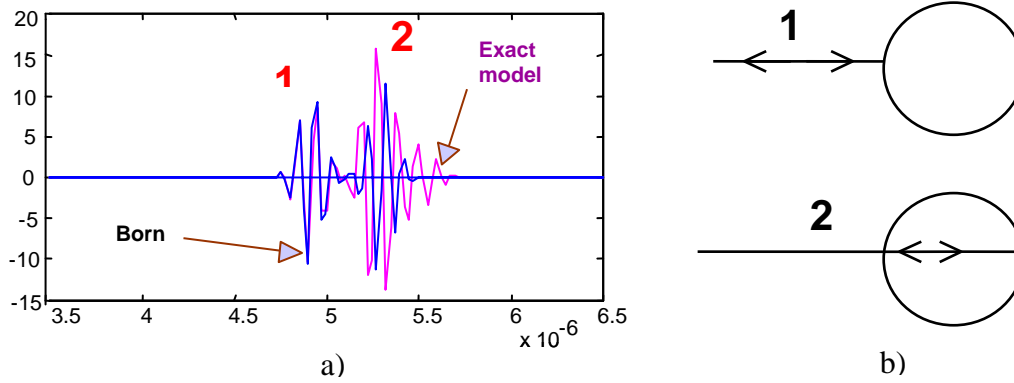


FIGURE 2. a) A-Scans modelled by Born (dark curve) and by Ying et Truell (bright curve) in the case of a nickel inclusion in copper ( $\frac{\delta\rho}{\rho}=0$  and  $\frac{\delta c_L}{c_L}=0.2$ ) b) Schematisation of echoes from reflections on the shining points : number 1 on the front surface and number 2 on the back surface.

We therefore reviewed such existing approaches and selected the Born and EQSA approximations. The Born approximation applied to elastodynamics [8,9] has been shown to be effective to model weak scattering [10]. This low frequency ( $ka < 1$ ) model consists in approximating fields inside the scatterer by the incident fields. This assumes small variations of the structural parameters between the host medium and the inclusion (density and elastic stiffness tensor). The extended quasistatic approximation (EQSA) [1] is a second low frequency approximation which mixes some assumptions of the Born approximation and of the static limit (accurate at very low frequency). The strain field inside the defect is replaced by the static field, calculated with incident fields supposed to be permanent while the displacement field inside the defect is approached by the incident field. In theory, validity frequency range of EQSA is larger than Born's one :  $ka < 1,5$  [1].

An exact analytical model, the so-called Ying and Truell model, is also available in the literature [2]. The solution is limited to spherical voids and inclusions.

In Figure 2, we show a comparison between simulated A-Scans obtained with CIVA by applying, for the beam-inclusion interaction, the Born approximation and Ying and Truell model. We observe that Born approximation induces an erroneous time delay between the reflections from the front 1 and back 2 flaw surfaces. This effect is also observed with EQSA approximation. So as to correct this effect and also some amplitude discrepancies, we have modified both Born and EQSA approximations by adding in the initial solutions a new assumption (called D<sup>2</sup>W) that amounts to take into account wave velocity and density differences between the matrix and the inclusion.

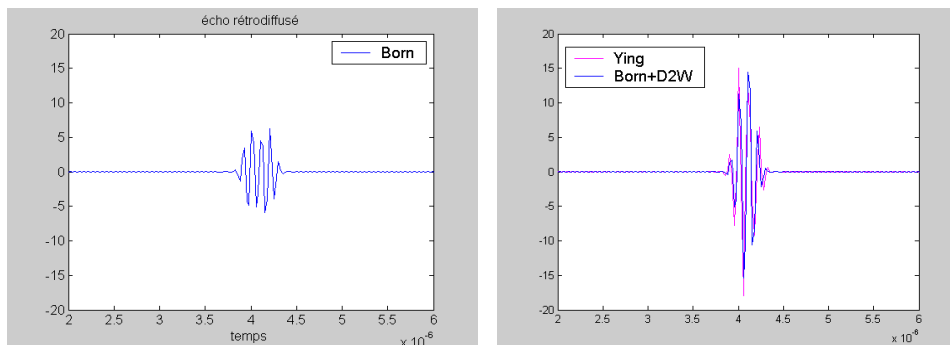


FIGURE 3. A-Scans of a  $\varnothing 560\mu\text{m}$  spherical alumina inclusion in steel inspected at 10 MHz ( $ka=3$ ) with the exact model (Ying : bright curve) and the approached models (Born and Born with D<sup>2</sup>W).

In order to illustrate the improvements reached by applying the D<sup>2</sup>W assumption we have simulated the response of a spherical alumina inclusion in steel which is characterized by important variations of structural parameters ( $\frac{\delta\rho}{\rho} = -0.5$  and  $\frac{\delta c_L}{c_L} = 0.89$ ). On Figure 3 are shown the comparisons between Ying and Truell, Born and Born + D<sup>2</sup>W results. In this example,  $ka = 3$ , a value inside our range of interest ( $1 < ka < 4$ ). The initial approached models (EQSA and Born) give rise to two separate echoes arising from the front and back surfaces which are not observed in Ying and Truell result. On the contrary, by adding to these two approximate models the D<sup>2</sup>W method, both amplitude and wave form are in a good agreement with the exact solution.

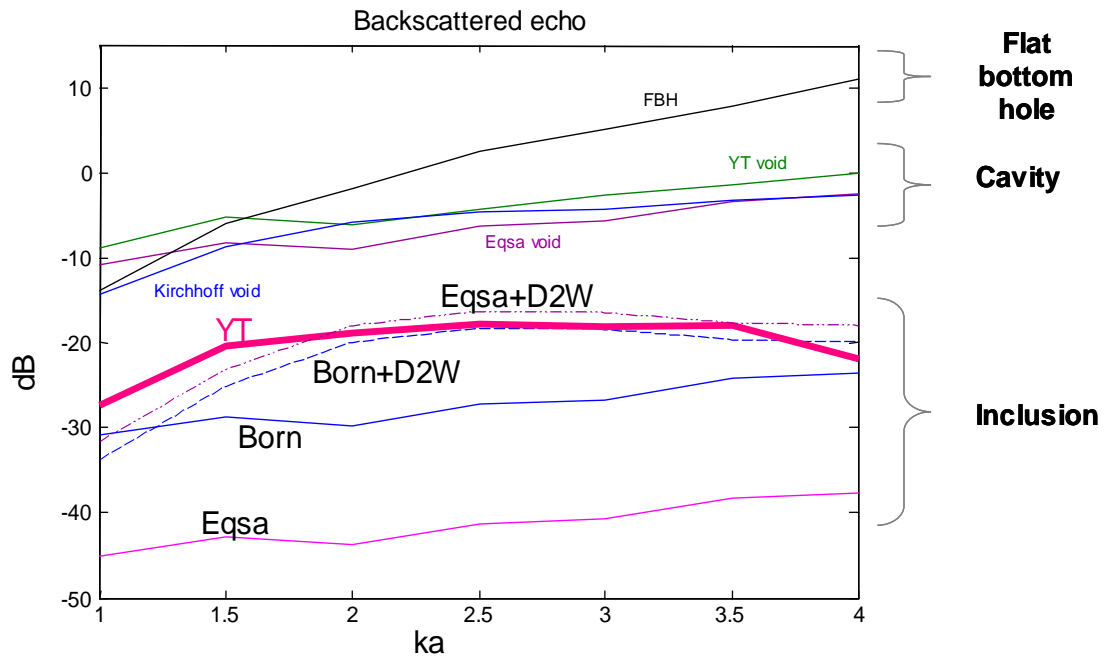


FIGURE 4. Echo amplitude versus  $ka$  for spherical alumina inclusions, flat bottom holes and spherical voids in steel.

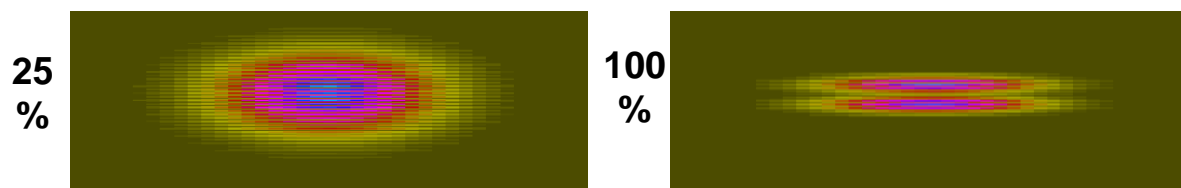


FIGURE 5. Influence of the bandwidth : inspection of a  $\varnothing 1,5$  mm diameter spherical inclusion.

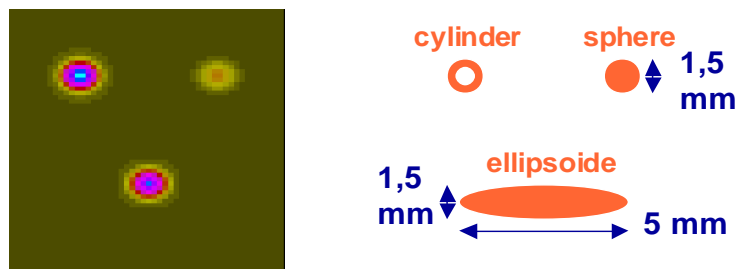


FIGURE 6. Influence of the flaw shape. Inspection of three alumina inclusions with different geometries : a  $\varnothing 1,5$  mm diameter sphere, a cylinder with height equal to diameter (1,5 mm) and an ellipsoid which differs from the sphere only by one diameter (5 mm).

A wide range of computations have been carried out in the aim of comparing the previously reported modelling approaches. Have been added in our study the high frequency Kirchhoff approximation which is applied in Mephisto code for dealing with voids. In Figure 4, is presented the amplitude versus  $ka$  curves of echoes arising from spherical alumina inclusions and voids, and flat bottom holes (FBH) in steel. Regarding voids, the comparison of Ying and Truell results with both EQSA and the high frequency Kirchhoff approximation shows a good agreement in our study range ( $1 < ka < 4$ ). Regarding the alumina inclusions, we can confirm that the application of  $D^2W$  quite improves the EQSA or Born approximation and the “exact” amplitudes (of the first echo when several) are well reproduced. These results have convinced us that the Born +  $D^2W$  and EQSA +  $D^2W$  reliability are quite equivalent in our domain of application. We therefore decided to adopt in Civa Born +  $D^2W$  approximation because of its capability of dealing with various flaws geometries.

In Figure 5 and Figure 6 are presented some examples of Bscans simulated by applying the Born +  $D^2W$  model illustrating the code capability. In Figure 5 are presented two results on a spherical inclusion showing the influence of the transmitted signal bandwidth on the possibility of distinguishing the reflections from the front and back surfaces. In Figure 6 are shown on the same result responses of inclusions of various geometries (cylindrical, ellipsoidal and spherical) : the cylinder gives rise to the most important echo owing to his plane face which is favourable to backscattering.

## EXPERIMENTAL VALIDATION

Experimental validations of the Born +  $D^2W$  model have been performed on both artificial and real inclusion-type defects. We have firstly created calibrated cylindrical inclusions by diffusion welding technique and spherical inclusions by hot isostatic pressing. We present, in Figure 7, results concerning two cylindrical inclusions with same diameter and length (2 mm and 5 mm) whose centre is located at a 17.5 mm depth. The axis of revolution of the flaws is the incidence axis of the transducer. The two echoes due to the reflection on the front and back surfaces of the cylinder are detected. Measurements have been carried out at different frequencies from 3.5 MHz to 15 MHz. On Figure 7 are plotted the amplitudes of the front surface echo measured at 3.5 MHz. The superimposition of these experimental data on the theoretical amplitude versus size curve obtaining by applying Born+ $D^2W$  model shows the reliability of the model predictions. A similar agreement (better than 3dB) has been obtained for all the  $ka$  values from 3.7 to 26.7. It is noteworthy that the agreement is necessarily better for lower  $ka$ .

We present also on Figure 8 comparisons between experimental and simulated wave forms. The agreement is quite good both at low frequency (3.5 MHz : Figure 8.a) and high frequency (15 MHz : Figure 8.b). We can observe at 15 MHz the amplitude loss between the two echoes due to attenuation in alumina. This phenomenon is taken into account in the model. The inputted attenuation parameters have been deduced from measurements carried out on alumina samples. These samples were identical to the artificial inclusions and immersed in water.

Strongly laminated stainless steel products containing natural alumina inclusions have also been investigated in the aim of validation of the model. The sample acquisition were performed at 50 MHz.

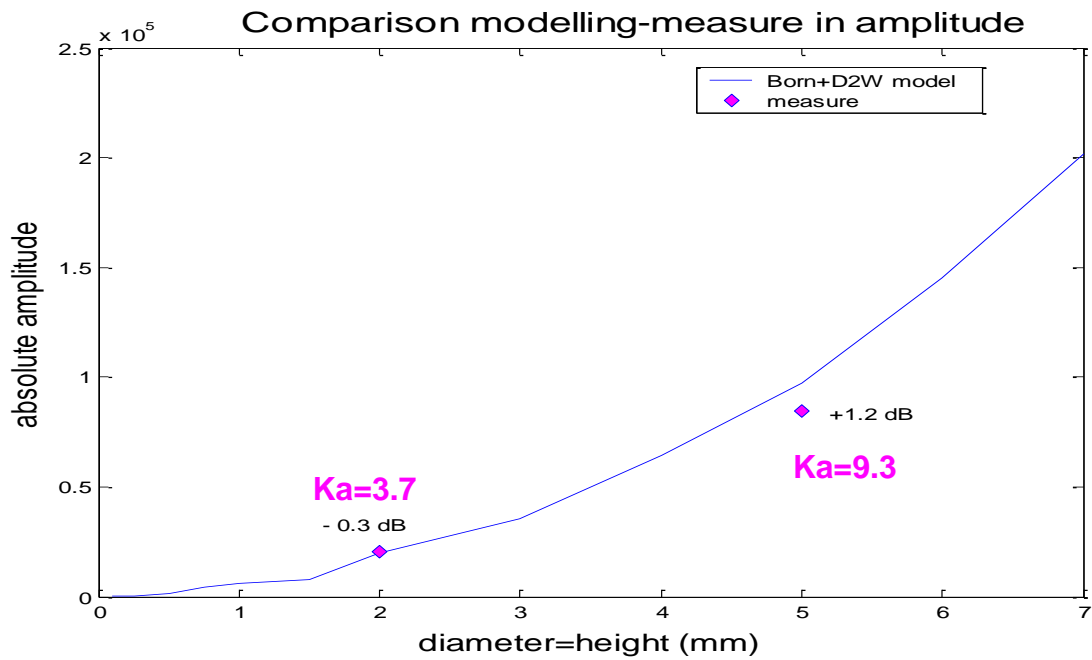


FIGURE 7. Comparison of the first echo amplitude between model and experiment on the cylindrical inclusions using a transducer 3.5 MHz focused at the flaw centres.

The results presented on Figure 9.a) concern an alignment of inclusions detected by ultrasonics and by X-rays measurements. The figure shows the superimposition of the ultrasonic Cscan and the corresponding X-rays view. From X-rays view have been deduced the size of inclusions assumed to be ellipsoidal which have been inputted in the model. We can see on Figure 9.b) the good agreement between the simulated and experimental Cscan; the amplitude discrepancy being less than 1 dB. These excellent results have to be confirmed by additional measurements on other defects.

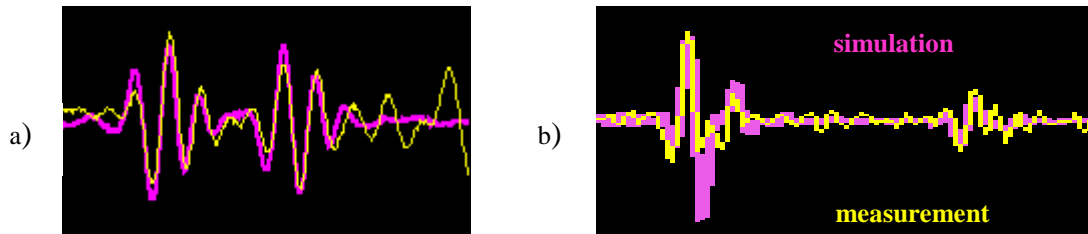


Figure 8. a) Comparison of the measured and simulated normalized wave forms for the  $\varnothing$  5 mm cylindrical inclusion at 3,5 MHz ( $ka=9.3$ ) b) idem at 15 MHz ( $ka=40.1$ ) .

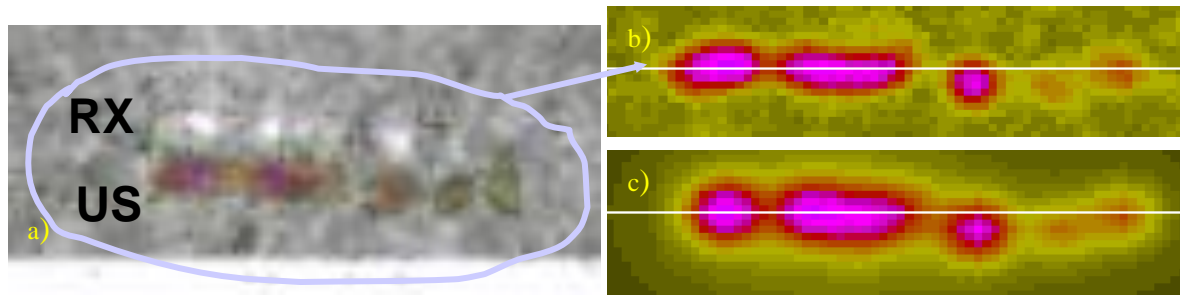


FIGURE 9. a) Superimposed experimental C-Scan and X radiography b) experimental C-Scan c) simulated C-Scan.

## CONCLUSIONS

To model the beam-inclusion interaction in Civa, we chose an approximated model to treat inclusions of different shapes (cylindrical, spherical, ellipsoidal) based on Born approximation. This model noted here Born+D<sup>2</sup>W accounts for wave velocity and density variations between the inclusion and host material.

This model has been extensively validated either theoretically by comparison with the Ying and Truell exact analytical solution available for spherical inclusions or experimentally.

The experiments have been performed on both artificial and real flaws and show a quite satisfactory agreement.

Work is now on progress for integrating to the theoretical predictions a modelling of the microstructural noise [11].

## REFERENCES

1. Gubernatis J.E. and Domany E., *J. Appl. Phys.* **50** (6), 4046 (1979).
2. Ying C.F. and Truell R., *J. Appl. Phys.* **27**, 1086 (1956).
3. L. Paradis, M. Talvard, Ph. Benoist, Ph. Rizo, et G. Bayon, *Review of Progress in Quantitative Non Destructive Evaluation*, 17B, Eds. D.O. Thompson and D.E. Chimenti, Plenum Press, N.Y., 1998, p.1981.
4. P. Calmon, A. Lhémery, I.Lecoeur-Taïbi, R. Raillon, 23<sup>rd</sup> *Rev. Prog. QNDE*, 16B, Eds. D.O. Thompson and D.E. Chimenti, Plenum Press, N.Y., 1997, p. 1861.
5. P. Calmon, A. Lhémery, I. Lecoeur-Taïbi, R. Raillon, L. Paradis, *Nuclear Engineering and Design* (1998).
6. S. Mahaut, O. Roy, S. Chatillon and P. Calmon, *Review of Progress in QNDE*, 21A, Eds. D.O. Thompson and D.E. Chimenti, Plenum Press, N.Y., 2001, p 894.
7. N. Gengembre, A.Lhémery, *Review of Progress in QNDE*, 21A, Eds. D.O. Thompson and D.E. Chimenti, Plenum Press, N.Y., 2001, p 815.
8. Gubernatis J.E., E. Domany, *J. Appl. Phys.* **48**, 2812 (1977).
9. Rose J.H. and Richardson J.M., *J. of Nondestructive Evaluation* **3** (1), 45 (1982).
10. Chiou C.P., Margetan F.J. and Thompson R.B., *Review of Progress in QNDE*, 15A, Eds. D.O. Thompson and D.E. Chimenti, Plenum Press, N.Y., 1996, p.49.
11. Chatillon S., Poidevin C. and Calmon P., *Review of Progress in QNDE*, Vol. 22 (these volumes), Eds. D.O. Thompson and D.E. Chimenti, Plenum Press, N.Y., 2002.